A remarkable CHF of 345 W/cm^2 is achieved in a wicked-microchannel using HFE-7100

Wenming Li[1, 2, *], Kai Luo[3], Chen Li[3] and Yogendra Joshi[2, *]

[1] Key Laboratory of Energy Thermal Conversion and Control of Ministry of Education, School of Energy and Environment, Southeast University, Nanjing, 210096, PR China
[2]George W. Woodruff School of Mechanical Engineering
Georgia Institute of Technology, Atlanta, 30332, USA
[3]Department of Mechanical Engineering,
University of South Carolina, Columbia, 29208, United States

***Corresponding e-mail:** wenmingli@seu.edu.cn; yogendra.joshi@me.gatech.edu

ABSTRACT: Boiling heat transfer of dielectric fluids is a promising cooling technique for thermal management of microelectronic systems. However, the critical heat flux achievable is generally low, because of the poor thermophysical properties of these fluids. To address this dilemma, we propose a new cooling concept to substantially enhance liquid supply during phase−change using enhanced capillary-driven force. Additionally, dedicated vapor pathways are designed among a bank of micro-pillars to facilitate vapor removal. In this work, new wicks comprised of silicon micro-pinfin arrays are explored to significantly enhance the flow boiling heat transfer performance. To examine the functionalities of this wick, experiments on HFE-7100 were carried out with mass velocities varying from 247 kg/m^{2}s to 3,465 kg/m^{2}s. To explore the enhancement mechanisms and to analyze the capillary-assisted flow boiling process, visualization studies were conducted. The results indicate that sustainable evaporation induced by wick microstructures and efficient liquid supply are the enhancement mechanisms compared to parallel microchannels with solid walls. It is found that the overall heat transfer coefficient is substantially increased up to 75%. A high critical heat flux (CHF) of approximately 345 W/cm^2 is recorded at G = 3,465 kg/m^{2}s at coolant inlet temperature of ~20 ^{o}C. Equally importantly, this noticeable enhancement of CHF value is associated with drastically decreased pressure drops compared to microchannels decorated with μ-pinfin fences.

KEYWORD: Capillary-assisted evaporation/boiling, Embedded cooling, Silicon wick, HFE-7100

Nomenclature

A	Area, m^2
C_p	Specific heat of water, kJ/kg·K
D_h	Hydraulic diameter, m
G	Mass flux, kg/m^2·s
h	Heat transfer coefficient, kW/m^2·K
H	Height, m
h_{fg}	Latent heat of vaporization, kJ/kg

k_s	Conductivity of silicon
K	Slope of linear function, Ω/K
L	Length, m
m	Parameter for fin efficiency
$\dot{m}$	Mass flow rate, kg/s
q''	Heat flux, W/cm^2
p	Pressure, N/m^2
Δp	Pressure drop, N/m^2
P	Power, W
R	Electrical resistance, Ω
t	Substrate thickness, m
T	Temperature, ^{o}C
$\bar{T}$	Average temperature, ^{o}C
W	Microchannel width, m
Greek symbols	
θ	Contact angle
μ	Viscosity, kg/(s·m)
ρ	Density, kg/m^3

σ	Surface tension, N/m
η_f	Fin efficiency
Subscripts	
a	Ambient
e	Exit
eff	Effective
i	Inlet
l	Liquid
o	Outlet
sat	Saturated
tp	Two-phase
v	Vapor

1. INTRODUCTION

Phase-change cooling techniques are of growing interest for the thermal management of high power density electronics. Due to safety considerations, dielectric fluids have attracted significant attention for direct contact thermal management. The low thermal conductivity and low surface tension typical of these coolants limit their heat transfer performance compared to fluids such as water. Surface modifications through nanowires [1-3] and hydrophilic coatings [4] might not be effective for dielectric fluids, since their low surface tension adversely impacts the stability of thin liquid film, deteriorating the heat transfer performance.

Surface modification through reentrant cavities [5] and other porous surfaces [6] are effective in improving the heat transfer rate through increasing evaporation and nucleate boiling by advancing liquid spreading. Additionally, channel size variation [7] and inclination [8] have been found to be important to enhance heat transfer in nucleate boiling. But high CHF values were rarely reported in the past studies carried out at room temperature ambient conditions. Easy dry-out due to lack of global rewetting is the main reason for this difficulty [9]. A high value of CHF was reported by Lee and Mudawar [10] for microchannel flow boiling of HFE-7100 by pre-cooling the coolant to -30 ˚C prior to the test section. At a flow rate of 5,550 kg/m^2 s, they achieved a maximum heat flux of ~700 W/cm^2 with a significant sensible heat component.

Two main factors are responsible for the difficulty in achieving enhanced CHF in flow boiling in micro-channels, without significant sub-cooling, explosive boiling, and dry-out. It is known that low fluid thermal conductivity will significantly decrease the heat transfer rate, resulting in significant increase of wall temperature. Hence, explosive boiling might occur as the heat input further increases. Also, the vapor sublayer on the heating surface induced by low surface tension usually happens at low CHF value on smooth surfaces [11, 12]. The techniques exploited in water for extending CHF such as bubble slugs regulation [13, 14], flow instability suppression [15, 16], surface modifications [2, 17-21], and rewetting enhancement [22-25] are not suitable for low surface tension dielectric coolants.

High heat transfer coefficient (HTC) and CHF, accompanied with reduced pumping power are highly desirable for efficient cooling. Hybrid liquid supply has been demonstrated by combining multiple jets and capillary cavities [26] to enhance both HTC and CHF. This study demonstrated that capillarity can be substantially increased by introducing micro/nanostructures. Wick microstructure comprised of pinfin fence was extensively investigated in microchannels of cross-section 220 um × 250 um with solid walls [27]. Superior heat transfer performance was demonstrated by rectifying two-phase flows. The significant generation of vapor was confined within channels, resulting in a significant increase of total pressure drop. With this issue in mind, porous wall made of micro-pinfin arrays were proposed to replace the solid walls in a microchannel of cross section 1.8 mm × 250 um to increase the porosity of the device [28, 29]. The porous wall was called wick in this study because it is assumed to function like wicks in heat pipes to facilitate the liquid flow through capillary action. Wick made of Polydimethylsiloxane (PDMS) was experimentally investigated to promote flow boiling of HFE-7100. To enhance vapor flow compared to conventional high-density wicks, dedicated vapor flow passages were introduced in the wick. The results using PDMS wick showed that capillary-assisted heat transfer was dominant. In the present study, wicked microchannel (aspect ratio of 7.2) was designed in silicon, based on the study of PDMS wick [29]. The heat transfer performance including HTC and CHF will be characterized using dielectric coolant HFE-7100. The pumping power shall be reduced by increasing the porosity to promote two-phase transport.

Table 1 The main thermophysical properties of HFE-7100 [9].

	μ (kg/m s)	**σ (mN/m)**	**c_p (kJ/kg K)**	**ρ (kg/m^3)**
Liquid (25 °C)	3.8×10^{-4}	13.6	1133	1481.6
Vapor (61 °C)	2.7×10^{-4}	N/A	N/A	10.535

2. FABRICATION OF DEVICE AND EXPERIMENTAL PROCESS

2.1. Rationale of design and fabrication

Table 1 lists the key thermophysical properties of HFE-7100. By comparison, they are significantly inferior to DI-water. Our prior study [28] has developed PDMS wick to compensate for these poor properties to enhance overall heat transfer performance. Figure 1 shows the schematic drawing of the tested chip and illustrates the rectangular arrangement of a silicon textured wick microstructure studied here. This wick is comprised of micro-pinfin array to form thin liquid film because of enhanced capillary effect. Vapor pathways are introduced into the wick to effectively direct the accumulated vapor flows. The dimensions (diameter, height) of micro-pillars are 30 μm and 250 μm, respectively. The pillar spacing is 10 μm and 25 μm in the axial direction (flow direction) and transverse direction (width), respectively. The width of vapor passage is 120 μm. The distance between two neighboring vapor pathways is 325 μm. This wicked microfluidic device is characterized with a porosity of 0.57. To indicate the sustained capability of fluid flow through the device, Figure 2 plots its permeability under different mass fluxes, which is nearly constant at about 2,6000 Darcy.

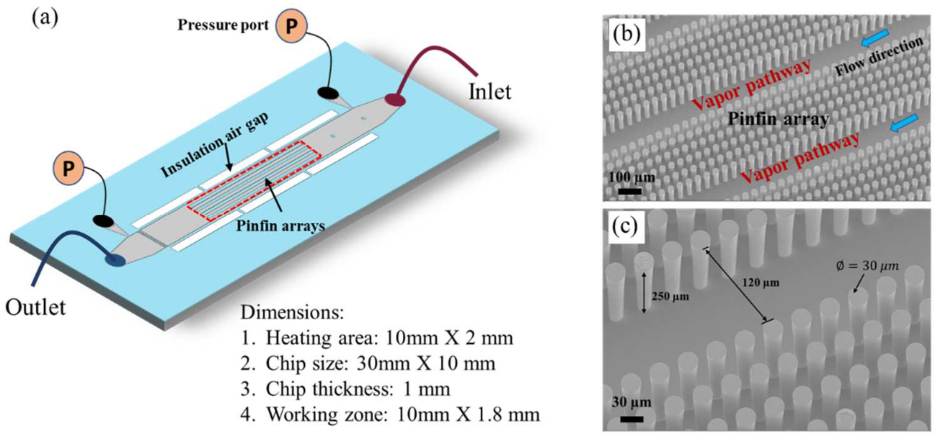

Figure 1 (a) The schematic drawing of the tested chip, including the main dimensions; (b)The Scanning Electron Microscope (SEM) image of the wicks and major dimensions. (c) Zoomed-in view of the wicks and vapor pathway. The capillary pressure between two neighboring micropillars ranges from 2.2 kPa to 5.4 kPa calculated by the equation $\Delta P = 4\sigma\cos\theta/D_h$. The contact angle θ is 0.

It is hypothesized that this wicked device comprised of micro-pillar arrays, with accompanying vapor pathways could effectively promote boiling heat transfer by significantly enhancing capillary-assisted boiling and evaporation [29]. Prior work has demonstrated the significant effect of porous surfaces made of copper inverse opals on capillary-assisted boiling [30]. Furthermore, HTC was substantially increased in a single silicon microchannel with high density micro-pillars [31]. But these dense micro-pillars resulted in large flow resistance, degrading the two-phase transport. Boiling crisis was triggered due to the vapor aggregation, leading to premature CHF. Thus, the enhancement of CHF was not significant. In contrast, efficient two-phase transport was demonstrated with short micro-pinfin arrays on the channel bottom [4]. In this way, the flow resistance was not increased since the infused-liquid film in short micro-pillars seems to act like a slip layer. Rewetting ability was the result of increased capillary effect. More recently, capillary μ-pinfin fences were found to have the ability to generate new two-phase boundary layers [32], enhancing two-phase transport. Sustainable thin film evaporation was maintained to achieve pronounced increase in HTC. In summary, simultaneous enhancement of HTC and CHF can be achieved by increasing the capillary flow using wicking effect, while vapor is efficiently removed from the device.

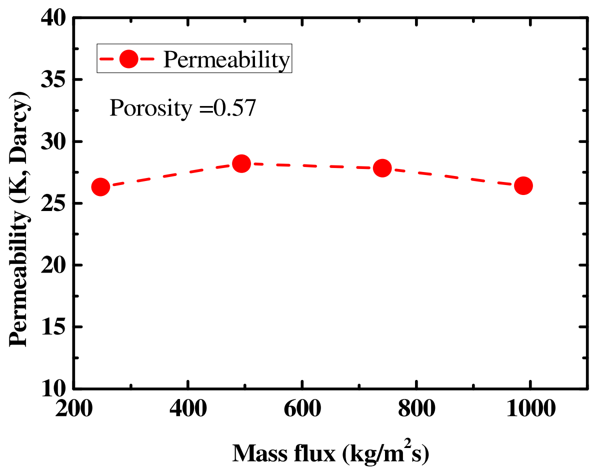

Figure 2 The permeability of this wick microstructure varies with mass flux. Permeability is

defined as: $K = \frac{Q \cdot A \cdot L}{\mu \cdot \Delta P}$, where Q is the volumetric flow rate, μ is the viscosity, ΔP is the pressure drop, A is the cross-sectional area, and L is the channel length.

Figure 3(a) schematically illustrates the working mechanisms of the explored concept. In a boiling process, thin liquid film will be potentially formed among the wicks. Because of pressure imbalance, vapor flow inside the wicks is directed into the vapor passages. With enhancement of vapor removal, thin film evaporation is promoted owing to enhanced capillary flow. Figure 3(b) experimentally demonstrated the formation of thin film. Furthermore, liquid-vapor menicus is assumed to be formed among the micro-pillars because of capillary effect. Two-phase heat transfer in wicks has been extensively studied [32, 33]. Higher evaporation rate usually occurs at the liquid-vapor meniscus [34, 35]. The improved liquid spreading because of increased capillary effect delays dryout, leading to higher CHF.

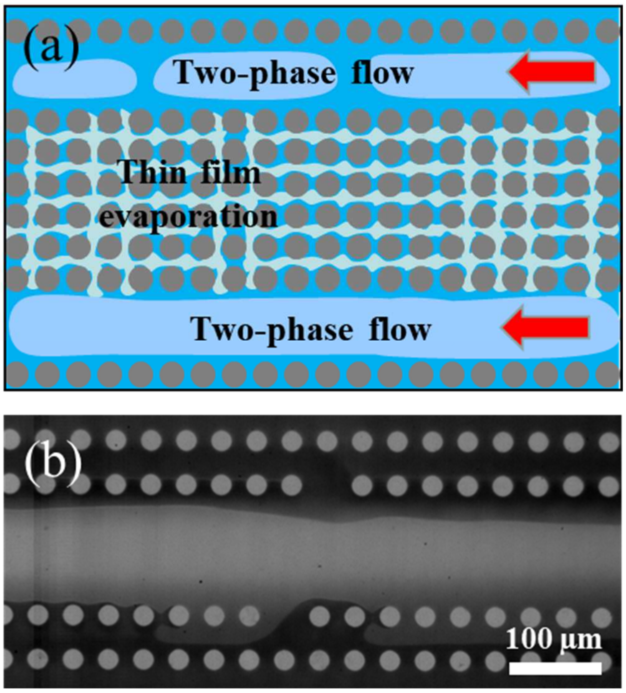

Figure 3 Working mechanism of structures studied is schematically and experimentally illustrated in top views: (a) schematic illustration of boiling/evaporation process. Thin film evaporation is facilitated by the wicks. (b) experimental observation of thin film formation for pillar diameter of 30 μm, pillar spacings of 10 μm and 25 μm in axial direction (liquid flow) and transverse direction, respectively, in a rectangular arrangement, heat flux of 45 W/cm^2, and mass flux of 247 kg/m^2 s.

To examine the thermal performance, a microdevice was fabricated on silicon substrate using microfabrication techniques in cleanroom. The tested device can function as a micro-evaporator. A micro-heater of dimensions (L, W) of 1 cm and 0.2 cm, with thickness of Aluminum metal film of about 0.8 μm was applied on the tested device to simulate the heat source. The pre-calibrated micro-heater also functioned as a resistance thermometer to measure average temperature, allowing the calculation of the average HTC for a prescribed heat input. Wicks were fabricated through deep reactive ion etching process. After this, a Pyrex glass wafer with a thickness of 0.5

mm was bonded to the etched silicon wafer using anodic bonding. Visualization studies were conducted to facilitate the analysis of boiling phenomena.

2.2. Experimental measurements

Figure 4 schematically illustrates the experimental arrangement used in this study. More details about the description of the key components can be found in our prior study [36]. The system includes a high-speed camera (maximum frame rate of 70,000 fps) mounted to the microscope, a data acquisition system, testing stage, and flow loop. Degassed HFE-7100 was pumped through the testing system by compressed nitrogen. Two pressure transducers were applied to collect inlet/outlet pressures. A Krohne Optimass 3300c flow meter was used to monitor the flow rates. A digital programmable power supply (BK-PRECISION XLN10014) was connected to the micro-heater. An Agilent digital multimeter was used to collect electrical signals. The room temperature was about 18 °C. The HFE-7100 was stored at room temperature before entering the test section. Heat loss was estimated prior to the experiments. Figure 5 plots the power loss that against heater temperature without coolant flow.

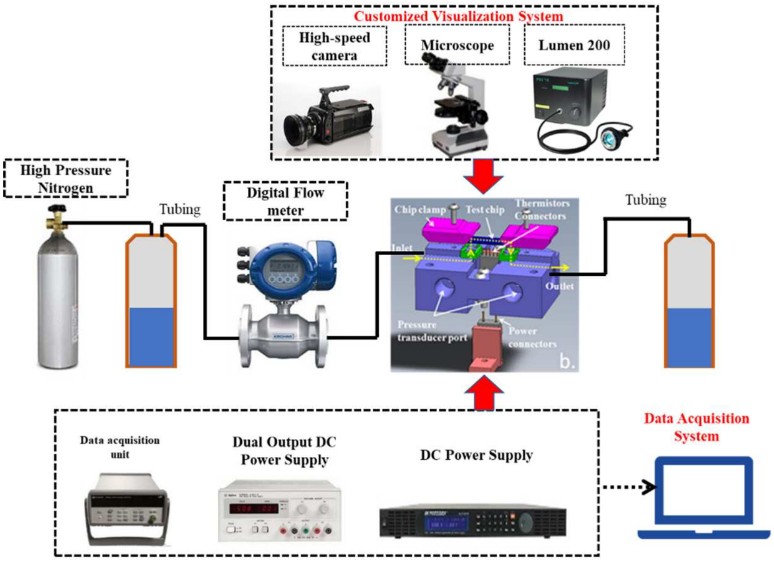

Figure 4 The experimental setup and the key components of the measurement system.

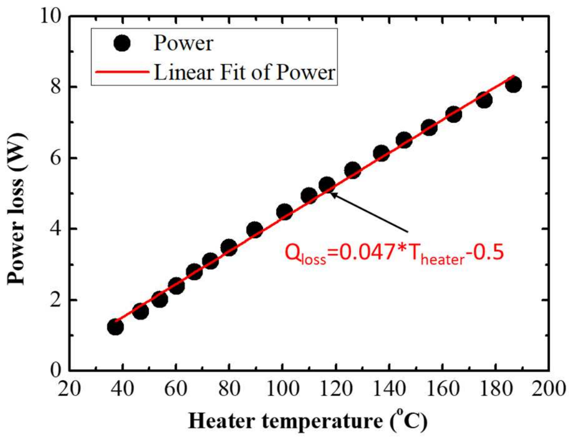

Figure 5 The power loss of the testing stage without coolant flow.

2.3. Data reduction

The aim of this section is to characterize the overall HTC, CHF, and exit vapor quality. To calculate the HTC, it is important to get the values of effective heat flux by subtracting heat loss (calibrated in Figure 5), resulting in

$$q''_{eff} = \frac{P - Q_{loss}}{A} \tag{1}$$

The heat is mainly dissipated through the latent and sensible component. Herein, latent heat is expressed as,

$$Q_{latent} = P - Q_{loss} - Q_{sensible} \tag{2}$$

On the other hand, the sensible heat is calculated by

$$Q_{sensible} = GA_c C_p \left(T_o - T_i\right) \tag{3}$$

The wall temperature of the tested device is used to obtain HTCs. Thus, pre-calibration of micro-heater was done prior to the experiments. The slope K allows calculation of the average heater temperature

$$\bar{T}_{heater} = K\left(R - R_a\right) + T_a \tag{4}$$

With this heater temperature, the average temperature of channel inner bottom surface is estimated as (neglecting spreading resistance):

$$\bar{T}_{wall} = \bar{T}_{heater} - \frac{q''_{eff} t}{k_s} \tag{5}$$

In this study, overall HTC is the result of effective heat flux divided by the superheat:

$$\bar{h} = \frac{P_{eff}}{A_b\left(\bar{T}_{wall} - T_{sat}\right)} \tag{6}$$

In microchannel, the pressure drop is usually substantial, indicating the saturation temperature (T_{sat}) of coolant will be influenced by the actual pressure. Thus, the calculation of saturation temperature is performed at the middle pressure within the channel, obtained as,

$$p = p_i - \frac{\Delta p}{2} \quad (7)$$

2.4. Uncertainty analysis

Table 2 shows uncertainties of main experimental variables. These values were estimated by using the approach of Kline and McClintock [37].

Table 2. Uncertainty of main experimental variables

Parameter	Uncertainty in tested range
V, DC Voltage	± (0.05%+25 mV)
A, Current	± (0.08%+0.1 mA)
Mass flux	± 0.1%>0.3 kg/h
Ambient temperature	± 1 °C
Pressure	± 0.25%
Pressure drops	± (0.35-0.50) kPa
Effective heat flux	± (< 6%)
Wall temperature	± (< 2.4 °C)
Overall HTC	±5.6%

3. RESULTS AND DISCUSSION

This section presents the characterization of two-phase transport as heat transfer coefficient, critical heat flux, and pressure drop. The enhancement mechanism will be discussed through comparisons between the current design and previously studied configurations as the baseline.

Visualization studies will be presented to assist the analysis of the results.

3.1. Flow boiling curves

Figure 6(a) shows boiling curves of the present wicked channel at three different flow rates. Three typical stages were observed in the boiling curves. Before the onset of bubble nucleation, the temperatures increased rapidly due to the low specific heat of HFE-7100. Subsequent to the onset of nucleate boiling (ONB), the slopes of the curves reduced owing to the significant contribution of latent heat of vaporization during the boiling process. With continued increase in heat flux, the trend of boiling curves changed again, possibly due to dryout in the outlet section because capillary flow reached its limit. Sudden increase of wall temperature is due to the extension of dryout spots toward to the inlet. Visualizations presented later support this interpretation.

To further characterize the boiling heat transfer, Figure 6(b) presents the overall HTCs derived from the data in Figure 6(a). The fin effect of channel sidewalls was not considered. Initially, the curves sharply decline against the heat fluxes. Around ~35 kW/m^2 K, the HTCs become more stable. We hypothesize that thin film evaporation was dominant at this condition in the entire channel until the occurrence of dryout.

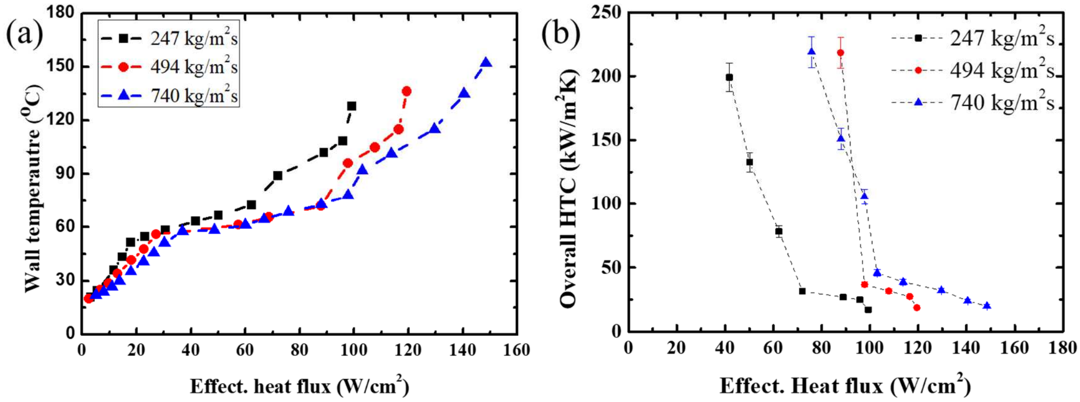

Figure 6 (a)The boiling curves of the present study and (b) the overall HTCs calculated by the base area.

3.2. Overall HTC enhancement

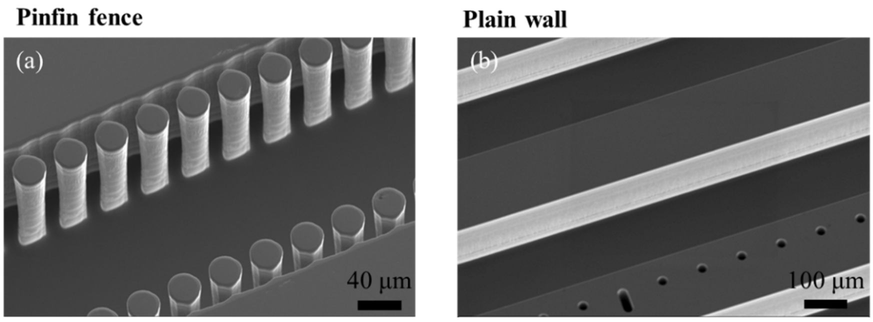

Figure 7 Two representative microchannel features were selected for comparison, including the base channel (plain wall) and microchannel with pinfin fences.

Comparison of average heat transfer rate was done to reveal the enhancement mechanism observed in the present design. Two representative microchannel features (in Figure 7) were selected for this comparison, including the base channel (plain wall) and microchannel with pinfin fences. Figure 8(a) presents the significant enhancement of HTC between the current study and that on plain wall microchannels. A high value near 140 kW/m^2 K is achieved at 240 kg/m^2s in the initial boiling region. The values for plain wall microchannels are much lower for the entire range. For comparison, Figure 8(b) illustrates the results of HTC for the developed boiling region. Noticeably, the enhancement is about 76%, much higher than that at the lower flow rate. Additionally, the difference in overall HTC between the current study and microchannel with pinfin fences is very small (about 5%) for the developed boiling region when thin film evaporation is dominant [38], as illustrated in Figure 9. But the values in the early boiling stage are much higher for the present configuration under the same effective heat fluxes condition, about three times. This may indicate that increased heat transfer area is essential to this enhancement. The solid walls in the prior microchannel configuration with pinfin fences [38] are completely replaced with micro-pillars on this design. Also, enhanced evaporation of meniscus induced by micropillar arrays should be an important factor for this significant difference in overall HTCs. One reported study has shown that trapped liquid bridges in the pore-throat structures can significantly enhance thin film evaporation [39].

Capillary micro-pinfin arrays employed here can facilitate the formation of thin liquid film between the pillars. In addition, this work also incorporates dedicated vapor passages to further promote the liquid supply to the wicks. Therefore, efficient thin film evaporation can be maintained. In striking contrast, the high density of micro pin-fin bundles [27]or pore-throat structures [39] without dedicated pathways significantly inhibits the vapor removal from the wicks. To conclude, the enhanced HTCs in this design are the combination effect of nucleation, convection, and thin film evaporation, which are the three main heat transfer components in microchannel flow boiling [26]. To show the advantages of hybrid rewetting mechanism in boiling heat transfer, Table 3 compares the current study with other reported studies on various designs, substrates, and coolants. Interestingly, the overall HTCs of this study ranges from 17 kW/m^2 K to 220 kW/m^2 K, much higher than that in others.

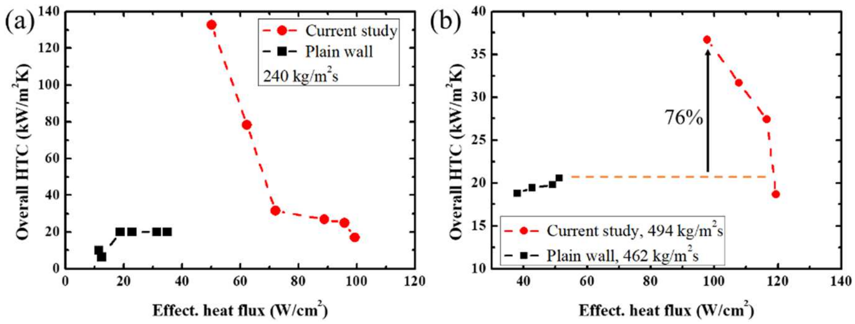

Figure 8 Overall HTC is significantly increased by ~76% over microchannels with solid walls [38].

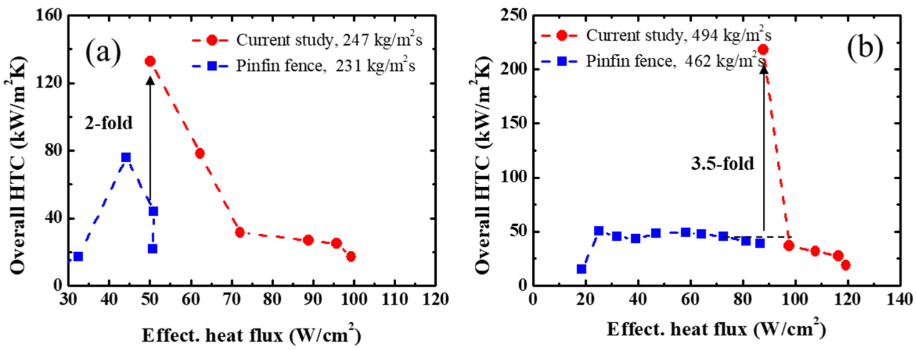

Figure 9 Enhanced overall HTC compared to pinfin fence [38].

Table 3 Comparisons of heat transfer performance between different reported studies on silicon/copper substrates.

References	**Dimensions (L, W, H)**	D_h **(μm)**	**Substrate material**	**Coolant**	**Mass flux (kg/m²s)**	**Overall HTC (kW/m²K)**	**CHF (W/cm²)**
Li et al [9]	Five-parallel channels, (10 mm, 200 μm, 250 μm)	222	Silicon	HFE-7100	231 ~ 2772	6~117	48~216
Alam et al [40]	Five-parallel channels, (10 mm, 200 μm, 250 μm)	222	Silicon	HFE-7100	400~1600	3~18	52~130
Al-Zaidi et al [41]	Twenty five-parallel channels, (25 mm, 700 μm, 350 μm)	466.7	Copper	HFE-7100	50~250	3~12.7	2.17~33.5
Lee and Mudawar [10]	Eleven-parallel channels, (10 mm, 205 μm, 1041 μm)	416	Copper	HFE-7100 T_{in}=-30 ˚C	6730	N/A	750

C.-J. Kuo [5]	Five-parallel channels, (10 mm, 200 μm, 250 μm)	222	Silicon	HFE-7000	264~3025	2~10	50~140.4
Present work	Single wicked channel, (10 mm, 1.8 mm, 250 μm)		Silicon	HFE-7100	247 ~3465	17~220	100~345

3.2.1. Enhanced capillarity

The main aim of this work is to noticeably increase the capillarity in dielectric coolants, via incorporation of wicks. Many studies have been reported to enhance the effect of capillarity on boiling heat transfer in dielectric fluids. For example, high density cavities were developed to maintain liquid film on heating surfaces [26]. Most recently, micro-porous structures were explored to trap liquid film with enhanced capillary effect to promote evaporation [39]. Furthermore, hybrid micro/nanoporous structures have been demonstrated to substantially enhance capillary flow [42]. However, these techniques impart high flow resistance for both liquid and vapor long-distance transport. In this work, Long-distance liquid transport is enabled with this design by combining increased capillary effect and vapor pathways. Figure 10 shows the time sequential images of capillary flow near the outlet section in the initial boiling stage for G = 247 kg/m^2 s and heat flux of 45 W/cm^2. This portion of channel experienced a periodic dryout-rewetting process. The rewetting velocity is about 0.2 m/s to quickly refresh the channel in a short duration. This process can lead to higher HTCs because of increased thin film evaporation compared to microchannels with solid walls, as shown in Figure 8 and Figure 9. Furthermore, in the middle section of this channel, sustainable thin liquid film was recorded for one rewetting cycle owing to enhanced capillary effect (in Figure 11).

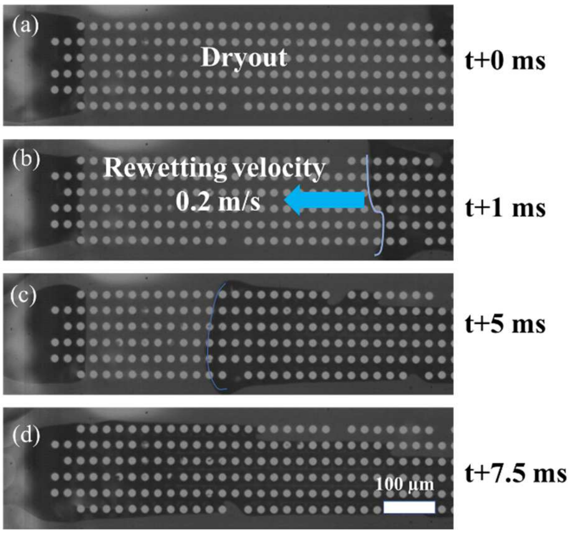

Figure 10 Time sequential optical images of capillary rewetting near outlet section at 247 kg/m^2 s and 45 W/cm^2.

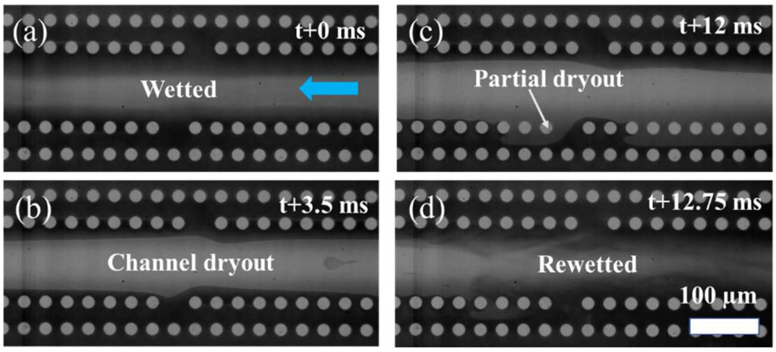

Figure 11 Sustainable thin liquid film in the middle of channel owing to enhanced capillary effect at 247 kg/m^2 s and 45 W/cm^2.

3.3. CHF enhancement

In larger channels, the values of CHF are primarily influenced by mass flux, vapor quality, pressure, hydraulic diameter, channel length, and thermophysical properties of coolants. This study explored the mechanisms of CHF enhancement in a single microchannel by embedding wick microstructures on HFE-7100. The values of CHF are mostly influenced by the capability of liquid supply. The present design aimed to solve this issue. Figure 12 shows a comparison between three different microchannel configurations to demonstrate a noticeable CHF enhancement in this work. Remarkably, a relatively high CHF, about 345 W/cm^2, is achieved on this configuration with a room for further enhancement at flow rates higher than 3,465 kg/m^{2}s. Table 3 also compares the CHFs of this design with other reported studies to show the advantage of hybrid liquid rewetting induced by the wicking microstructures and the dedicated vapor pathways.

The observed enhancements are about 1.8-fold and 1-fold compared to plain wall and μ-pinfin fences, respectively, at G = 240 kg/m^{2}s. When mass velocities increase to about 1,600 kg/m^{2}s, this enhancement decreases to about 90% compared to plain wall. These considerable enhancements are the result of multiple factors. Firstly, the flow pathways provide passages for both vapor and liquid transport through the micro-device. Therefore, liquid can be pumped to the entire wicks in a timely fashion (in Figure 10), delaying the CHF crisis. Secondly, local liquid spreading is substantially improved through the integration of wick microstructures that significantly increase the capillarity. Figure 11 shows the ability of this design to sustain liquid film in the wicks because of enhanced capillary effect. The comparison in Figure 12 indicates that silicon wick comprised of capillary micro-pillar arrays significantly outperforms the other two configurations in terms of CHF. The CHF enhancements are more significant in the present configuration at lower flow rates (below 1,600 kg/m^{2}s). The efficient utilization of coolant through the entire wicks is attributed to this. At high flow rates (above 1,600 kg/m^{2}s), the inertial force acting on the two-phase interfaces is much larger. A small portion of wicks near the inlet section didn’t function well. Hence, the enhancement decreases slightly compared to other two configurations.

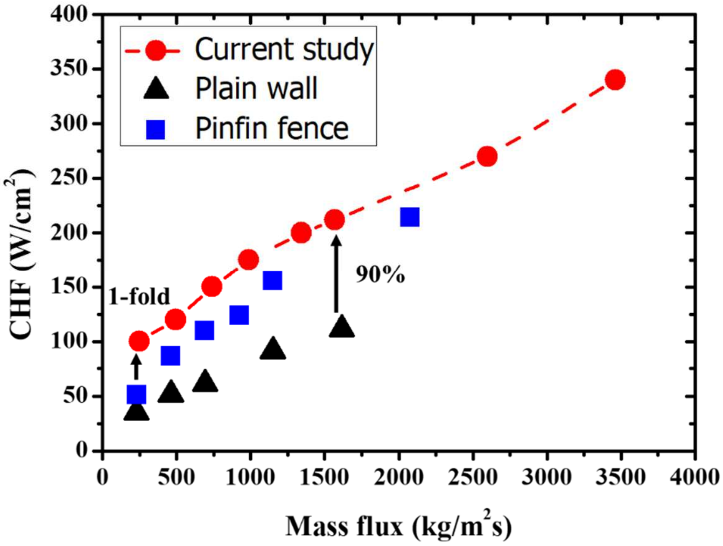

Figure 12 Significant enhancement of CHF compared to smooth wall and micro-pinfin fences microchannels (illustrated in Figure 7). A relatively high CHF of 345 W/cm^2 is demonstrated for a mass velocity of 3,465 kg/m^{2}s.

Heating surface dryout or explosive boiling might be the main factors for the sharp decline of heat transfer rate as CHF is approached. Flow instabilities, for example two-phase oscillations, are believed to be the third factor because they induce liquid supply and rewetting crisis. In plain-wall microchannels, explosive boiling usually happens in dielectric fluids such as HFE-7100 because of their low thermal conductivity [43]. Inverted annular flow regime was observed in HFE-7100 with vapor layer forming on the heating surfaces [9]. Explosive boiling and dry-out crisis has been mitigated in microchannels integrated with capillary micro-pinfin fences because of rapid liquid renewal and improved liquid spreading [43]. In this study, the dedicated vapor pathways further improve the local liquid spreading through the wicks, which is another reason for the CHF enhancement. Approaching CHF conditions, Figure 13 shows that dryout occurred in the middle and outlet sections of channel. The significant CHF enhancement was demonstrated by managing or addressing dryout or explosive boiling in the current design. The wick microstructures can potentially avoid explosive boiling at increased heat transfer rates.

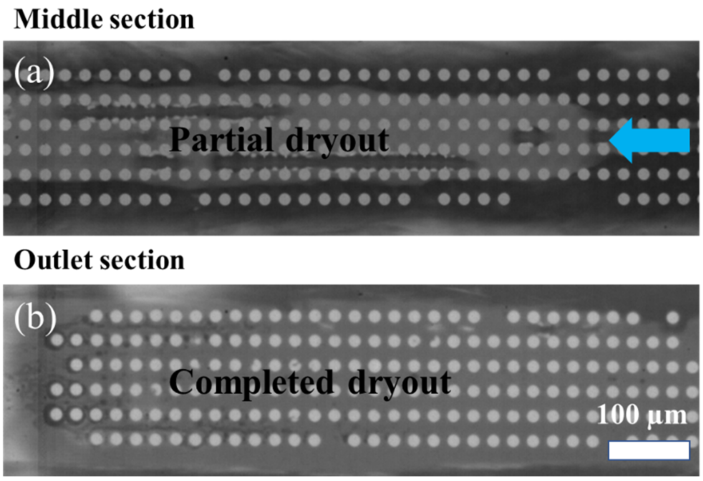

Figure 13 Dryout occurred in (a) the middle section and (b) outlet section of channel near CHF conditions.

3.4. Significant reduction of ΔP

Usually, enhancement of flow boiling heat transfer is associated with a significant increase in pressure drop, for example, enhancement using orifices [13] or high flow rates [44]. In this study, ability of two-phase transport (indicated by the high permeability) is noticeably improved by replacing the solid walls in conventional parallel microchannels with micro-pillar arrays. Enhanced flow boiling of HFE-7100 is demonstrated accompanying with significant reduction of two-phase pressure drops. Figure 14 plots the measured pressure drops across this as-fabricated channel. To show the advantage of this design in managing pressure drops while enhancing heat transfer performance, Figure 15 shows considerable reduction in two-phase pressure drops compared to that of microchannels decorated with pinfin fences. Interestingly, two-phase pressure drop is substantially reduced up to 57% at relatively higher heat input of 50 W/cm^2. This significantly reduced pressure drop is realized through efficient removal of vapor via the dedicated pathways. Note that the porosities of both designs are almost the same, about 0.57. This comparison proves the effectiveness of the present configuration in managing the two-phase pressure drops, while significantly enhancing the HTC and CHF.

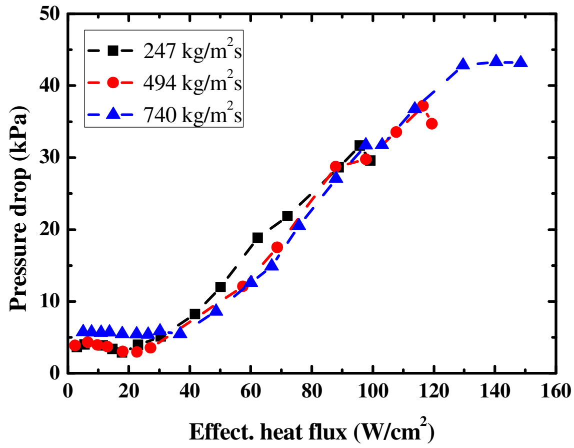

Figure 14 The measured pressure drops as a function of effective heat flux.

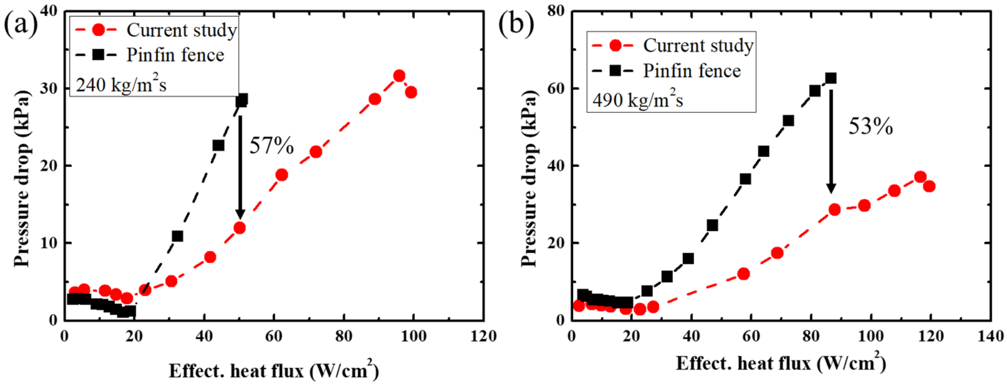

Figure 15 Measured pressure drops are decreased significantly compared to that of μ-pinfin fences.

4. CONCLUSION

A remarkable CHF of 345 W/cm^2 is demonstrated in a single wicked microchannel using HFE-7100 at G = 3,465 kg/m^{2}s. Significant enhancement of CHF, up to 1.8 times, is also demonstrated compared to plain-wall microchannels and pinfin fenced microchannels. The visualization studies illustrate that capillary-assisted evaporation is dominant by embedding wick microstructures. It is noted that vapor passage design not only has vital effect on the enhancement of CHF, but also in considerably reducing two-phase pressure drops, compared to pinfin fenced microchannels. The efficient heat transfer rate is the result of sustainable thin film evaporation. Finally, hybrid liquid supply and rewetting are demonstrated to be two key factors for the simultaneous enhancements of flow boiling. This novel design is promising for the cooling of high power microsystems, while reducing the pumping power.

ACKNOWLEDGEMENTS

The information, data, or work presented herein was funded in part by the Advanced Research Projects Agency-Energy (ARPA-E), U.S. Department of Energy, under Award Number DE-AR0001023 for Y.J. and W.L. at the Georgia Institute of Technology. The support for C.L. at the University of South Carolina was under the award of N000141612307 funded by the U.S. Department of Defense, Office of Naval Research (ONR) (Program Officer Dr. Mark Spector).

REFERNCE

[1] F. Yang, W. Li, X. Dai, C. Li, Flow boiling heat transfer of HFE-7000 in nanowire-coated microchannels, Applied Thermal Engineering, 93 (2016) 260-268.

[2] C. Li, Z. Wang, P.I. Wang, Y. Peles, N. Koratkar, G.P. Peterson, Nanostructured copper interfaces for enhanced boiling, Small, 4(8) (2008) 1084-1088.

[3] R. Chen, M.C. Lu, V. Srinivasan, Z. Wang, H.H. Cho, A. Majumdar, Nanowires for enhanced boiling heat transfer, Nano letters, 9(2) (2009) 548-553.

[4] Y. Zhu, D.S. Antao, K.-H. Chu, S. Chen, T.J. Hendricks, T. Zhang, E.N. Wang, Surface Structure Enhanced Microchannel Flow Boiling, Journal of Heat Transfer, 138(9) (2016) 091501.

[5] C.J. Kuo, Y. Peles, Flow Boiling of Coolant (HFE-7000) Inside Structured and Plain Wall Microchannels, Journal of Heat Transfer, 131(12) (2009) 121011.

[6] J.Y. Chang, S.M. You, Boiling heat transfer phenomena from microporous and porous surfaces in saturated FC-72, International Journal of Heat and Mass Transfer, 40 (1997) 4437-4447.

[7] K.-S. Yang, Y.-R. Jeng, C.-M. Huang, C.-C. Wang, Heat Transfer and Flow Pattern Characteristics for HFE-7100 Within Microchannel Heat Sinks, Heat Transfer Engineering, 32(7-8) (2011) 697-704.

[8] C.-C. Wang, W.-J. Chang, C.-H. Dai, Y.-T. Lin, K.-S. Yang, Effect of inclination on the convective boiling performance of a microchannel heat sink using HFE-7100, Experimental Thermal and Fluid Science, 36 (2012) 143-148.

[9] W. Li, J. Ma, T. Alam, F. Yang, J. Khan, C. Li, Flow boiling of HFE-7100 in silicon microchannels integrated with multiple micro-nozzles and reentry micro-cavities, International Journal of Heat and Mass Transfer, 123 (2018) 354-366.

[10] J. Lee, I. Mudawar, Fluid flow and heat transfer characteristics of low temperature two-phase micro-channel heat sinks – Part 1: Experimental methods and flow visualization results, International Journal of Heat and Mass Transfer, 51(17-18) (2008) 4315-4326.

[11] G. Hetsroni, A. Mosyak, E. Pogrebnyak, Z. Segal, Explosive boiling of water in parallel micro-channels,

International Journal of Multiphase Flow, 31(4) (2005) 371-392.
[12] L.V.Z. Yusheng Dou, Nicholas Winograd, and Barbara J. Garrison, Explosive Boiling of Water Films Adjacent to Heated Surfaces-A Microscopic Description, Journal of Physics Chemistry A, 105 (2001) 2748-2755.
[13] A. Koşar, C.-J. Kuo, Y. Peles, Suppression of Boiling Flow Oscillations in Parallel Microchannels by Inlet Restrictors, Journal of Heat Transfer, 128(3) (2006) 251.
[14] G. Wang, P. Cheng, A.E. Bergles, Effects of inlet/outlet configurations on flow boiling instability in parallel microchannels, International Journal of Heat and Mass Transfer, 51(9-10) (2008) 2267-2281.
[15] C.J. Kuo, Y. Peles, Local measurement of flow boiling in structured surface microchannels, International Journal of Heat and Mass Transfer, 50(23-24) (2007) 4513-4526.
[16] A. Kalani, S.G. Kandlikar, Combining liquid inertia with pressure recovery from bubble expansion for enhanced flow boiling, Applied Physics Letters, 107(18) (2015) 181601.
[17] N. Singh, V. Sathyamurthy, W. Peterson, J. Arendt, D. Banerjee, Flow boiling enhancement on a horizontal heater using carbon nanotube coatings, International Journal of Heat and Fluid Flow, 31(2) (2010) 201-207.
[18] A.K.M.M. Morshed, F. Yang, M. Yakut Ali, J.A. Khan, C. Li, Enhanced flow boiling in a microchannel with integration of nanowires, Applied Thermal Engineering, 32 (2012) 68-75.
[19] A. Sitar, I. Golobic, Heat transfer enhancement of self-rewetting aqueous n-butanol solutions boiling in microchannels, International Journal of Heat and Mass Transfer, 81 (2015) 198-206.
[20] M.S. Sarwar, Y.H. Jeong, S.H. Chang, Subcooled flow boiling CHF enhancement with porous surface coatings, International Journal of Heat and Mass Transfer, 50(17-18) (2007) 3649-3657.
[21] S.M. You, J.H. Kim, K.H. Kim, Effect of nanoparticles on critical heat flux of water in pool boiling heat transfer, Applied Physics Letters, 83(16) (2003) 3374-3376.
[22] H. O'Hanley, C. Coyle, J. Buongiorno, T. McKrell, L.-W. Hu, M. Rubner, R. Cohen, Separate effects of surface roughness, wettability, and porosity on the boiling critical heat flux, Applied Physics Letters, 103(2) (2013) 024102.
[23] B.S. Kim, H. Lee, S. Shin, G. Choi, H.H. Cho, Interfacial wicking dynamics and its impact on critical heat flux of boiling heat transfer, Applied Physics Letters, 105(19) (2014) 191601.
[24] D.E. Kim, S.C. Park, D.I. Yu, M.H. Kim, H.S. Ahn, Enhanced critical heat flux by capillary driven liquid flow on the well-designed surface, Applied Physics Letters, 107(2) (2015) 023903.
[25] K.-H. Chu, R. Enright, E.N. Wang, Structured surfaces for enhanced pool boiling heat transfer, Applied Physics Letters, 100(24) (2012) 241603.
[26] W. Li, X. Qu, T. Alam, F. Yang, W. Chang, J. Khan, C. Li, Enhanced flow boiling in microchannels through integrating multiple micro-nozzles and reentry microcavities, Applied Physics Letters, 110(1) (2017) 014104.
[27] A. Koşar, C. Mishra, Y. Peles, Laminar Flow Across a Bank of Low Aspect Ratio Micro Pin Fins, Journal of Fluids Engineering, 127(3) (2005) 419.
[28] Y. Joshi, W. Li, Wick-assisted evaporation for EV internal permanent magnet (IPM) motor drive cooling, U.S. Provisional Patent No. 63/018 987, (2020).
[29] W. Li, Y. Joshi, Capillary-Assisted Evaporation/Boiling in PDMS Microchannel Integrated with Wicking Microstructures, Langmuir : the ACS journal of surfaces and colloids, 36(41) (2020) 12143-12149.

[30] C. Zhang, J.W. Palko, M.T. Barako, M. Asheghi, J.G. Santiago, K.E. Goodson, Enhanced Capillary-Fed Boiling in Copper Inverse Opals via Template Sintering, Advanced Functional Materials, 28(41) (2018) 1803689.
[31] S. Krishnamurthy, Y. Peles, Flow boiling of water in a circular staggered micro-pin fin heat sink, International Journal of Heat and Mass Transfer, 51(5-6) (2008) 1349-1364.
[32] W. Li, Z. Wang, F. Yang, T. Alam, M. Jiang, X. Qu, F. Kong, A.S. Khan, M. Liu, M. Alwazzan, Y. Tong, C. Li, Phase-Change Heat Transfer: Supercapillary Architecture-Activated Two-Phase Boundary Layer Structures for Highly Stable and Efficient Flow Boiling Heat Transfer (Adv. Mater. 2/2020), Advanced Materials, 32(2) (2020) 2070013.
[33] S. Bigham, A. Fazeli, S. Moghaddam, Physics of microstructures enhancement of thin film evaporation heat transfer in microchannels flow boiling, Scientific reports, 7 (2017) 44745.
[34] X. Dai, L. Tran, F. Yang, B. Shi, R. Yang, Y.C. Lee, C. Li, Characterization of Hybrid-Wicked Copper Heat Pipe, in: ASME/JSME 2011 8th Thermal Engineering Joint Conference, 2011.
[35] X. Dai, F. Yang, R. Yang, Y.-C. Lee, C. Li, Micromembrane-enhanced capillary evaporation, International Journal of Heat and Mass Transfer, 64 (2013) 1101-1108.
[36] F. Yang, X. Dai, C.-J. Kuo, Y. Peles, J. Khan, C. Li, Enhanced flow boiling in microchannels by self-sustained high frequency two-phase oscillations, International Journal of Heat and Mass Transfer, 58(1-2) (2013) 402-412.
[37] S.J. Kline, F.A. McClintock, Describing uncertainties in single-sample experiments, Mechanical Engineering, 75(1) (1953) 3- 8.
[38] W. Li, Z. Wang, F. Yang, T. Alam, M. Jiang, X. Qu, F. Kong, A.S. Khan, M. Liu, M. Alwazzan, Y. Tong, C. Li, Supercapillary Architecture-Activated Two-Phase Boundary Layer Structures for Highly Stable and Efficient Flow Boiling Heat Transfer, Advanced materials, 32(2) (2020) e1905117.
[39] H. Hu, P. Jiang, F. Huang, R. Xu, Role of trapped liquid in flow boiling inside micro-porous structures: pore-scale visualization and heat transfer enhancement, Science Bulletin, 66(18) (2021) 1885-1894.
[40] T. Alam, W. Li, W. Chang, F. Yang, J. Khan, C. Li, A comparative study of flow boiling HFE-7100 in silicon nanowire and plainwall microchannels, International Journal of Heat and Mass Transfer, 124 (2018) 829-840.
[41] A.H. Al-Zaidi, M.M. Mahmoud, T.G. Karayiannis, Flow boiling of HFE-7100 in microchannels: Experimental study and comparison with correlations, International Journal of Heat and Mass Transfer, 140 (2019) 100-128.
[42] Y. Wang, Y. Lin, G. Yang, J. Wu, Flow Physics of Wicking into Woven Screens with Hybrid Micro-/Nanoporous Structures, Langmuir : the ACS journal of surfaces and colloids, 37(7) (2021) 2289-2297.
[43] W. Li, C. Li, Z. Wang, Y. Chen, Enhanced flow boiling in microchannels integrated with supercapillary pinfin fences, International Journal of Heat and Mass Transfer, 183 (2022) 122185.
[44] A. Kaya, M.R. Özdemir, A. Koşar, High mass flux flow boiling and critical heat flux in microscale, International Journal of Thermal Sciences, 65 (2013) 70-78.